Available online at www.sciencedirect.com

ScienceDirect

journal homepage: www.elsevier.com/locate/he

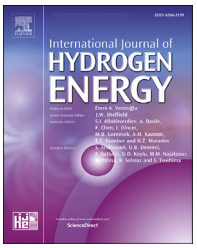

Heterogeneous cobalt phosphides nanoparticles anchored on carbon cloth realizing the efficient hydrogen generation reaction

Bai Xiang Tao [a], *Cui Ye* [a], *Xiao Lin Li* [a], *Xiao Hu Wang* [a], *Guo Chen* [a], *Ling Jie Li* [b], *Hong Qun Luo* [a,**], *Nian Bing Li* [a,*]

[a] *School of Chemistry and Chemical Engineering, Southwest University, Chongqing 400715, People's Republic of China*

[b] *School of Chemistry and Chemical Engineering, Chongqing University, Chongqing 400044, People's Republic of China*

ARTICLE INFO

Article history:
Received 24 August 2018
Received in revised form
14 October 2018
Accepted 1 November 2018
Available online xxx

Keywords:
Intrinsic activity modifying
Ultrafine size
Heterogeneous cobalt phosphides nanoparticles
Hydrogen evolution reaction

ABSTRACT

Intrinsic activity modifying of electrocatalysts is crucial to realizing the excellent catalytic performance towards hydrogen evolution reaction. Herein, we demonstrate a highly efficient electrocatalyst based on heterogeneous cobalt phosphides nanoparticles. The ultrafine size of the as-prepared catalyst (~5 nm) ensures the efficient extension of active sites. Furthermore, the incorporation of orthorhombic CoP and Co_2P contributes to the improvement of the inherent catalytic property. As a consequence, the as-prepared heterogeneous cobalt phosphides nanoparticles supported on carbon cloth exhibit impressive electrocatalytic activity, which only acquire a small overpotential of 90 mV at a current density of 10 mA cm^{-2}, and present a low Tafel slope (67.9 mV dec^{-1}), a large exchange current density (0.58 mA cm^{-2}) as well as good durability. Therefore, this work provides a favorable guidance for exploring executable strategies to improve catalyst activity.

Introduction

The excessive depletion of fossil fuels has led to many terrible issues, such as the global warming and "energy crisis". Therefore, the urgency of developing eco-friendly and renewable energy sources attracts a large number of researchers to explore in the energy-related fields [1–4]. Hydrogen, due to its high-energy density and pollution-free combustion products, has been considered as an ideal energy carrier to replace exhaustible traditional energy in the future [5–8]. Electrochemical water-splitting is acknowledged to be the simplest method to gathering high-purity hydrogen, while it always requires highly active catalysts to decrease the overpotential and increase the reactive rate towards hydrogen evolution reaction (HER) [9–11]. Considerable studies have manifested that Pt group metals show excellent HER performance in acidic medium, but their large-scale applications are restricted due to their high economic cost and low abundance [12,13]. It is reported that the abundance of expensive Pt is about 3.7×10^{-6}% in the earth, which is orders of magnitude smaller than that of other non-precious metals including

* *Corresponding author*. Tiansheng Road, BeiBei District, Chongqing, 400715, People's Republic of China.
** *Corresponding author*. Tiansheng Road, BeiBei District, Chongqing, 400715, People's Republic of China.
E-mail addresses: luohq@swu.edu.cn (H.Q. Luo), linb@swu.edu.cn (N.B. Li).

https://doi.org/10.1016/j.ijhydene.2018.11.018
0360-3199/

Please cite this article as: Tao BX et al., Heterogeneous cobalt phosphides nanoparticles anchored on carbon cloth realizing the efficient hydrogen generation reaction, International Journal of Hydrogen Energy, https://doi.org/10.1016/j.ijhydene.2018.11.018

cobalt [14,15]. Toward this end, developing non-noble and highly efficient HER electrocatalysts is still a pressing and challenging task [16–18].

Eye-catching transition-metal chalcogenides (TMDs), which exhibit outstanding HER catalytic activity, have been vastly explored over the past years, such as MoS_2 [19,20], $CoSe_2$ [21,22], and NiS_2 [23,24]. Due to the high conductivity and low-cost, the nickel-based compounds have already been widely applied as HER electrocatalysts [25]. Unfortunately, it is reported that they are usually unstable in highly acidic solutions [26–28]. Transition-metal phosphides (TMPs), as the rising star in transition-metal-based HER catalysts, are usually used in the hydrodesulfurization (HDS) reaction, and the similar mechanism between HDS and HER further suggests that the HDS catalysts are more likely to serve HER [29,30]. Lots of reported studies about TMPs have claimed their outstanding HER performance [31–34]. For example, our group recently reported that the carbon framework wrapped cobalt phosphide (Co_2P@C/CC) can act as a flexible and efficient electrocatalyst in hydrogen evolution process [35].

Cobalt phosphides, as one of the typical TMPs, are regarded as the promising HER catalyst alternatives, which mainly benefit from their proper hydrogen adsorption energy (ΔG_H) [36]. It is reported that the appropriate molar ratio of Co and P is conducive to obtaining the higher current density under lower overpotential, which further contributes to the outstanding catalytic activity [37]. In addition, diverse morphologies of cobalt phosphides, including nanoparticles (NPs), nanosheets (NSs), and nanowires (NWs), as well as hollow nanostructures [30,38], have been studied. For example, Sun's group synthesized various CoP nanostructures and demonstrated that CoP nanowires exhibit the best HER catalytic activity [39]. Although numerous studies have been reported, it is inescapable to accept the research challenges associated with the adjustment of catalytic active phase of cobalt phosphides.

In this work, we are confident to design a nanocatalyst based on heterogeneous cobalt phosphides nanoparticles (Co_xP NPs) through two facile steps, which take advantage of the weak reflux process of cobalt acetate, followed by low-temperature gas-solid transformation strategy in the presence of PH_3 [40,41]. It is interesting to note that the as-prepared Co_xP NPs are made up of ultrafine Co_2P and CoP nanoparticles. Remarkably, when the Co_xP NPs supported on carbon cloth is used as a cathode catalyst in 0.5 M H_2SO_4, it only achieves current densities of 100 and 10 mA cm^{-2} at overpotentials of 168 and 90 mV, respectively. The influence of active phase on the catalytic activity is also systematically surveyed through providing the electrochemical data of comparative material (CoP NPs). Our study suggests that the modulation of inherent catalytic activity plays a crucial role in boosting catalytic efficiency.

Experimental section

Materials

All chemical reagents and solvents are of analytical reagent grade and used as received. $Co(Ac)_2 \cdot 4H_2O$ was purchased from Sinopharm Chemical Reagent Co. Ltd. (Ningbo, China). $NH_3 \cdot H_2O$, NaH_2PO_2, and anhydrous ethanol were obtained from Aladdin Industrial Co. Ltd. (Shanghai, China). Carbon cloth (CC) was bought from Wuhan Instrument Surgical Instruments Business (China).

Synthesis of the Co_3O_4 NPs/CC precursor

In a typical process, $Co(Ac)_2 \cdot 4H_2O$ (100 mg) was ultrasonically dissolved in 3 mL of ultrapure water to form a homogenetic solution, and then the above pink solution was added to 40 mL of anhydrous ethanol under magnetic stirring. After stirring for about 10 min, the violet solution was obtained and kept steady. Then $NH_3 \cdot H_2O$ (28 wt %, 1 mL) was introduced dropwise, and the color of the solution became dark green. Next, a typical reflux process was conducted in our work. In detail, the mixed solution was added to a round flask (120 mL) and kept stirring at 80 °C for 12 h. After the mixture cooled down naturally, it was transferred into a 100 mL polytetrafluoroethylene autoclave containing a piece of clean CC (1.5 cm × 1.0 cm), then sealed and heated at 160 °C for 3 h. Note that the CC was preprocessed with acetone, alcohol, and ultrapure water for each 30 min through sequential sonication. After the autoclave cooled down to room temperature, the Co_3O_4 NPs/CC precursor was taken out and treated with ultrapure water to remove excess species, followed by vacuum dried at 60 °C overnight.

Synthesis of the Co_xP NPs/CC catalyst

To obtain the heterogeneous Co_xP NPs/CC catalyst, the Co_3O_4 NPs/CC precursor was treated with a thermal phosphorylation process in the presence of NaH_2PO_4. Typically, NaH_2PO_4 (500 mg) was put in a porcelain boat and kept at the upstream side of the furnace, while the Co_3O_4 NPs/CC precursor was placed at the downstream side. Subsequently, with a heating rate of 5 °C min^{-1}, the system was heated to 300 °C and kept for 2 h under an ultrapure N_2 atmosphere. After the system cooled to room temperature, the Co_xP NPs/CC catalyst was rinsed with 1 M H_2SO_4 to dissolve the excess impurities and then rewashed with ultrapure water, followed by vacuum dried at 60 °C overnight. The mass loading of the Co_xP NPs/CC catalyst is about 1.3 mg cm^{-2} after several washes, measured by using a high-precision electronic balance. The preparation of pure phase CoP NPs/CC was consistent with the former except that the reaction temperature rose to 400 °C.

Synthesis of the CoP NPs/CC catalyst

The preparation of pure phase CoP NPs/CC was consistent with that of the Co_xP NPs/CC catalyst except that the amount of phosphorus source (NaH_2PO_4) was increased to 1 g and the reaction temperature rose to 400 °C.

Characterizations

The phase structures of the catalyst were characterized using X-ray diffraction (XRD, Bruker D8 ADVANCE) with Cu-Ka source radiation (λ = 1.54178 Å) at a scan rate of 2° min^{-1}. The Raman spectrum was obtained from a Renishaw (UK)

Please cite this article as: Tao BX et al., Heterogeneous cobalt phosphides nanoparticles anchored on carbon cloth realizing the efficient hydrogen generation reaction, International Journal of Hydrogen Energy, https://doi.org/10.1016/j.ijhydene.2018.11.018

using a 532.8 nm laser source. Scanning electron microscope (SEM) images of the as-prepared catalyst were performed on a Hitachi S-4800 field emission scanning electron microscope. A high-resolution JEM-ARM200F transmission electron microscope (TEM) was used to investigate the microstructure and obtain the corresponding energy dispersive X-Ray (EDX) spectra. X-ray photoelectron spectroscopy (XPS) analyses were performed with a Thermal ESCALAB 250 spectrometer.

Electrochemical measurements

Electrochemical tests were performed on a computer-controlled workstation (CHI660E, China) using a standard three-electrode system. Normally, the as-prepared Co_xP NPs supported on carbon cloth were used as a working electrode and a saturated calomel electrode (SCE) as the reference electrode. An inert Pt foil was used for the counter electrode when conducted the short-term activity tests, such as cyclic voltammetry (CV) and linear sweep voltammetry (LSV) tests. While a graphite rod was used when carrying out the stability tests. The SCE was first calibrated in 0.5 M H_2SO_4 saturated with high-purity hydrogen using two platinum-foils as the working electrode and the counter electrode, respectively (Fig. S1 in Supporting Information). To prepare the Pt/C ink catalyst, 20% commercial Pt/C powder (6 mg) was dissolved in 250 μL of ultrapure water containing 10 μL of Nafion. Then, 50 μL of Pt/C ink was spread on the clean CC (1.5 cm^2) and dried at room temperature. Before the electrochemical measurements, the electrolyte solution (0.5 M H_2SO_4) was bubbled with pure nitrogen for 30 min to remove the dissolved oxygen. The polarization curves were collected using the LSV measurement at a scan rate of 2 mV s^{-1}, and the sweeping potential range was from −0.8 to 0 V *vs.* SCE at room temperature. Note that all the polarization curves in our work were iR compensation. Electrochemical impedance spectroscopy (EIS) tests were conducted over a frequency range from 0.01 Hz to 100 KHz. Electrochemical stability was measured using continuous cyclic voltammetry scanning and the sweeping potential range was from −0.20 to +0.10 V *vs.* RHE at room temperature. In addition, a long-term chronoamperometry was also conducted to evaluate the durability of the resultant catalyst.

Results and discussion

Fig. 1 depicts the preparation process of the heterogeneous Co_xP NPs/CC. First, a simple reflux process to cobalt acetate was conducted under a mild condition, and subsequent hydrothermal oxidization accelerated the crystallization of Co_3O_4 NPs. Frequently-used carbon cloth acted as the substrate to support our samples. The Co_3O_4 NPs/CC precursor was then thermally treated in a low-temperature phosphorization process. The morphology and size of the as-prepared sample were observed by SEM and TEM. The SEM image of Co_3O_4 NPs/CC sample is displayed in Fig. 2B. Compared to the bare CC (Fig. 2A), it is obvious that countless ultrafine nanoparticles tightly adhere to the CC. Fig. 2D shows a typical TEM image of Co_3O_4 NPs, which can be observed that the nanoparticles were dispersed homogeneously and uniformly. The statistical analysis (inset in Fig. 2D) provides the information that the sizes of nanoparticles range from 3 to 8 nm. The formation of such tiny nanoparticles mostly benefits from weak hydrolysis under a mild condition and further weak oxidation of cobalt acetate, which will ensure a higher density of HER active sites [34]. Furthermore, the more detailed microstructure of Co_3O_4 NPs was observed by high-resolution TEM (HRTEM) and selected-area electron diffraction (SAED). As displayed in Fig. 2E, the HRTEM image shows a legible lattice spacing of 0.244 nm, indexed to Co_3O_4 (311) crystal plane. The SAED pattern (Fig. 2F) also shows the well-identified (311) crystal plane. All the above results indicate ultrafine Co_3O_4 NPs were successfully synthesized through mild reflux process.

It is reported that low-temperature energy-saving transformation tactics have no effect on the surface appearance [42,43], the SEM image of Co_xP NPs/CC after thermally treated with gas-phase phosphatization (Fig. 2C) also suggests that the ultrafine morphology is undamaged. Furthermore, the TEM image (Fig. 2G) and size distribution map (inset in Fig. 2G) also testify the above result. Fig. 2H depicts the HRTEM image of Co_xP NPs. Two clear lattice fringes with a spacing of 0.376 and 0.330 nm can be attributed to (020) and (101) crystallographic plane of Co_2P and CoP, respectively. The corresponding SAED pattern also confirms the heterogeneous structure of the resultant sample. As seen in Fig. 2I, the (020) plane of Co_2P and the (101) plane of CoP are well-identified. When the amount of phosphorus source and the reaction temperature were increased, the pure phase CoP NPs/CC catalyst was obtained. The SEM and TEM images of CoP NPs/CC are displayed in Fig. S2 A and B. Finally, the EDX spectra (Fig. S3) further confirm the presence of Co and P elements.

The X-ray diffraction (XRD) and Raman measurements were performed in order to identify the composition and phase of our samples. Fig. 3A shows the XRD pattern of the Co_3O_4 NPs, and three major diffraction peaks at 31.6°, 37.2°, and 65.7° can be definitely observed, which are indexed to the (011), (210), and (031) planes of cubic phase Co_3O_4 (JCPDS No. 65-3103). After thermal phosphatization procedure, the XRD pattern of the as-prepared CoP and Co_xP NPs is presented in Fig. 3B. For the CoP NPs, the noticeable diffraction peaks at 31.6°, 36.3°, 46.2°, and 48.1° are well-matched with the

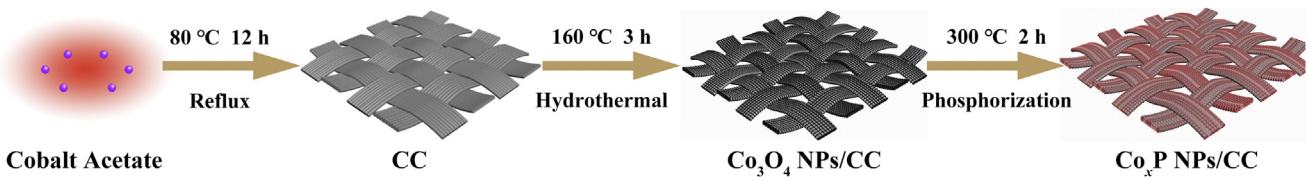

Fig. 1 – Schematic illustration of Co_xP NPs/CC preparation using Co_3O_4 NPs/CC as the precursor.

Please cite this article as: Tao BX et al., Heterogeneous cobalt phosphides nanoparticles anchored on carbon cloth realizing the efficient hydrogen generation reaction, International Journal of Hydrogen Energy, https://doi.org/10.1016/j.ijhydene.2018.11.018

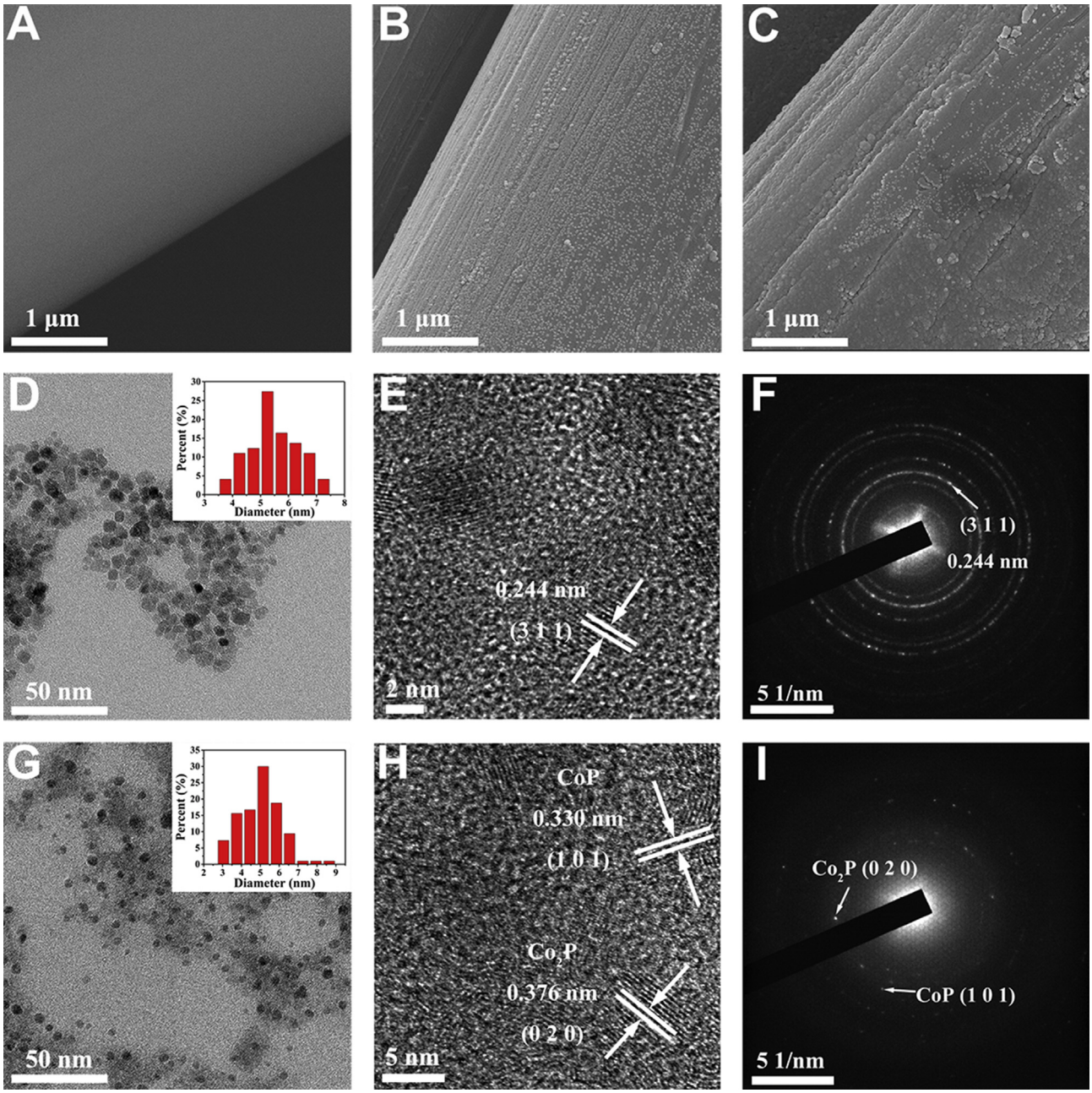

Fig. 2 – Morphology characterization. SEM images of (A) bare CC, (B) Co_3O_4, and (C) Co_xP NPs. (D and G) TEM, (E and H) HRTEM images and (F and I) SAED patterns of Co_3O_4 and Co_xP NPs. The insets of (D and G) show the size distribution maps of Co_3O_4 and Co_xP NPs, respectively.

standard cards of orthorhombic CoP (JCPDS No. 29-0497). While for the Co_xP NPs, other strong peaks at 40.7°, 40.9°, and 43.3° can be readily assigned to the (121), (201), and (211) planes of Co_2P (JCPDS No. 32-0306). This unusual phenomenon may be caused by the higher molar proportion of Co and lower reaction temperature (300 °C) in the progress of phosphorization, which further leads to the production of the heterogeneous phase of phosphides. No other miscellaneous peaks are observed in these XRD patterns, implying the successful synthesis of Co_3O_4 and Co_xP NPs. Furthermore, the Raman spectra displayed in Fig. S4 also confirm the above phenomenon. The Raman peaks of Co_3O_4 NPs observed at 188, 471, 510, 600, and 665 cm^{-1} correspond to five characteristic Raman vibration modes of Co_3O_4. There are no clear peaks for the as-prepared Co_xP NPs, which is accordance with the data of pervious study [44]. The XRD data and Raman analysis give a favorable evidence to demonstrate the high crystallinity of Co_3O_4 and Co_xP NPs in our work.

In order to determine the elemental constitution and the valence state of constituent elements in the as-prepared CoP and Co_xP NPs, the XPS measurement was performed in this study. According to the full scan spectral data of Co_xP NPs displayed in Fig. S5, the peaks indexed to the elements of O, C, P, and Co are easily identified. In addition, the detailed XPS

Please cite this article as: Tao BX et al., Heterogeneous cobalt phosphides nanoparticles anchored on carbon cloth realizing the efficient hydrogen generation reaction, International Journal of Hydrogen Energy, https://doi.org/10.1016/j.ijhydene.2018.11.018

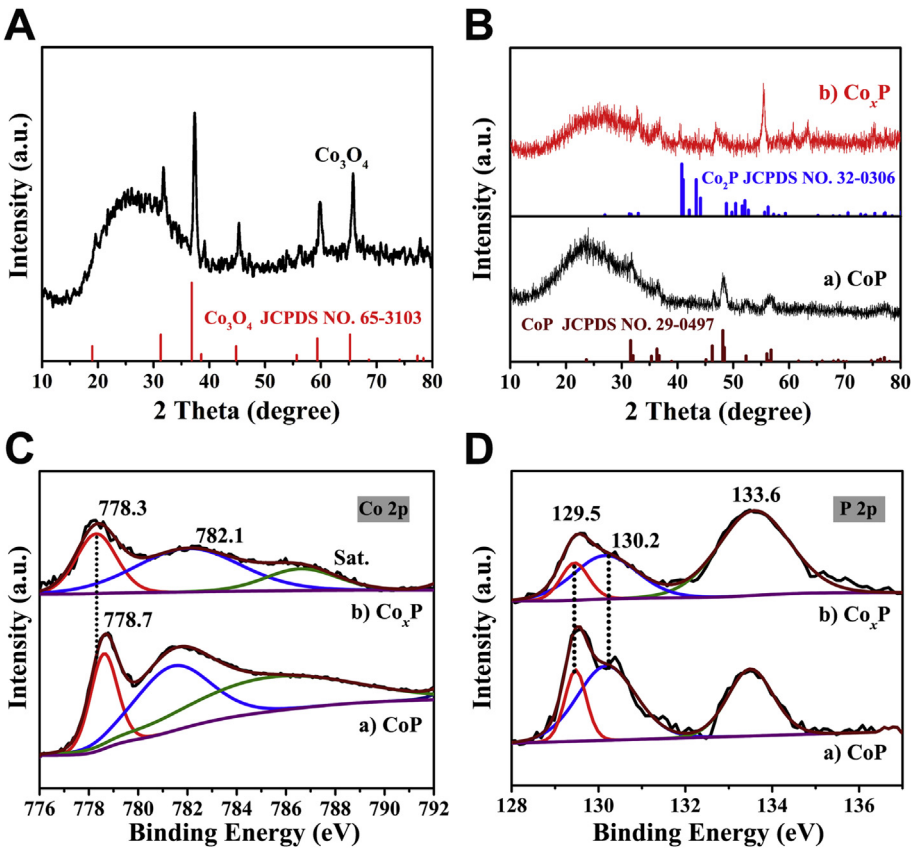

Fig. 3 – Structure and composition characterization. Powder XRD patterns of the as-prepared (A) Co_3O_4, (B) CoP and Co_xP NPs. High-resolution XPS spectra of (C) Co $2p_{3/2}$ and (D) P 2p for CoP and Co_xP NPs.

survey has also been carried out. Fig. 3C–b shows the high-resolution XPS spectrum of Co $2p_{3/2}$ core-level for Co_xP NPs, which can be easily fitted into three peaks. The peak located at 778.3 eV is attributed to the Co $2p_{3/2}$ of Co species in Co_xP NPs, corresponding to the XRD analysis [45]. Another peak at 782.1 eV is assigned to the Co^{2+} and Co^{3+}, and an obvious satellite peak is related to the shakeup excitation of the high-spin Co ions in the Co_xP catalysis [46,47]. Fig. 3D–b shows the high-resolution XPS spectrum of P 2p for Co_xP NPs. The peaks with binding energy at 129.5 and 130.2 eV can be ascribed to the P $2p_{3/2}$ and P $2p_{1/2}$ of P species in the Co_xP, while the peak at 133.6 eV is allocated to the P–O bond [48]. Oxide appears in the final product, which can be ascribed to the slight superficial oxidation of Co_xP under the atmosphere environment [49]. Notably, the binding energy of Co $2p_{3/2}$ (778.3 eV) is quite close to that of metallic Co (777.9 eV), and the value of P $2p_{3/2}$ is slightly lower than that of elemental P (130.0 eV). The above data indicate that the reduced Co species have partial positive charge, and demonstrate the existence of a negative charged P species, suggesting the presence of electron density transformation from Co to P, which is perfectly consistent with the previous study [37,45]. In addition, the XPS data of as-obtained CoP NPs have also been investigated (Fig. 3C–a and Fig. 3D–a). Compared to the XPS data of Co_xP NPs, the fitting peak of Co $2p_{3/2}$ (778.7 eV) for CoP NPs positively shifted, implying a smaller cobalt valence state in targeted Co_xP NPs.

The electrocatalytic performance of the Co_xP NPs and CoP NPs adhering to the CC was assessed in the 0.5 M H_2SO_4 solution through a typical three-electrode configuration. For comparison, the catalytic activity of the commercial Pt/C was also examined. The polarization curves of the above different materials are presented in Fig. 4A. Obviously, the commercial Pt/C exhibits the lowest overpotential, which means the excellent HER activity. Under similar test condition, the pure phase CoP NPs/CC shows higher overpotentials of 150 and 223 mV for the current densities of 10 and 100 mA cm^{-2}. Noticeably, the overpotentials required to drive the current densities of 10 and 100 mA cm^{-2} on the as-prepared heterogeneous Co_xP NPs/CC catalysts are only 90 and 168 mV, respectively. The overpotential value is lower than that of the pure phase CoP NPs/CC and most reported non-noble metal HER catalysts (Table S1), indicating its outstanding catalytic performance towards HER.

Furthermore, in order to survey the probable kinetics of HER, Tafel plots were also estimated by plotting overpotential (η) against the logarithm of current density (j). Fig. 4B exhibits the Tafel slopes of Pt/C, Co_xP NPs/CC, and CoP NPs/CC. Through fitting the linear part of the Tafel plot, a slope of 37.9 mV dec^{-1} for the Pt/C is observed, which is in accordance with the reported value [50]. The Tafel slope of the pure phase CoP NPs/CC is 92.3 mV dec^{-1}, while the heterogeneous Co_xP NPs/CC exhibits a smaller Tafel slope of 67.9 mV dec^{-1}, indicating an easier catalytic process towards HER. The values of Tafel slope for all catalysts are in the range of 40–120 mV dec^{-1}, insinuating a Volmer-Heyrovsky HER mechanism in this study [51]. Furthermore, by applying the extrapolation

Please cite this article as: Tao BX et al., Heterogeneous cobalt phosphides nanoparticles anchored on carbon cloth realizing the efficient hydrogen generation reaction, International Journal of Hydrogen Energy, https://doi.org/10.1016/j.ijhydene.2018.11.018

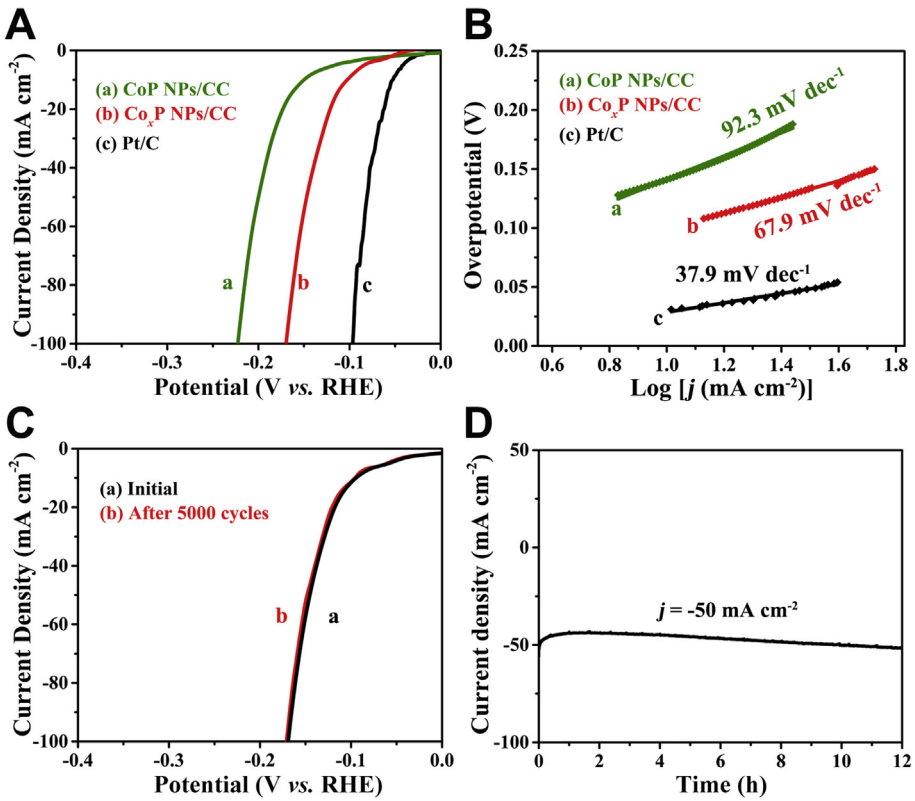

Fig. 4 – (A) Polarization curves recorded for CoP NPs/CC, Co_xP NPs/CC, and Pt/C in 0.5 M H_2SO_4. (B) Tafel plots for the CoP NPs/CC, Co_xP NPs/CC, and Pt/C. (C) Polarization data for Co_xP NPs/CC before and after 5000 CV scanning cycles. (D) Time dependence of the current density for the Co_xP NPs/CC at a static overpotential of 150 mV.

method to the Tafel plot, the exchange current density of Co_xP NPs/CC is calculated to be 0.58 mA cm^{-2} (Fig. S6), which is relatively large among some non-noble metal HER catalysts listed in Table S1.

The above phenomena suggest an improved catalytic activity of the as-prepared Co_xP NPs/CC in contrast to the pure phase CoP NPs/CC catalyst, which can be benefited from the simple intrinsic activity modifying of electrocatalysts. Furthermore, such outstanding catalytic performance may be explained as follows. Firstly, the cooperative effect of the Co_2P and CoP in heterogeneous Co_xP species enhances the intrinsic catalytic property and electron transport rate of the cobalt phosphides. According to previous calculations and experiments, both the transition metal and P atoms in the TMPs play important roles in boosting HER activity [45]. In this work, Co_xP NPs with diverse Co species realized the successful modification of inherent catalytic activity on some level. Secondly, the ultrafine morphology of the as-prepared Co_xP NPs/CC not only enables the more exposure of catalytic active sites but also ensures the maximized utilization for reactants. Lastly, Co_xP NPs tightly contacting with CC assist stable chemical and electronic connection and further favor the mobility of electrons between CC and Co_xP NPs during hydrogen generation reaction.

The stability in strong acidic medium is of extraordinary importance for the catalysts used in obtaining hydrogen from water. Therefore, we conducted a series of accelerated aging tests to evaluate the durability and recyclability, such as continual CV scanning and a long-term chronoamperometry. Notably, recently increasing researchers reported that using noble Pt foil as the counter electrode is unable to determine the catalysts stability precisely, because metal Pt can be dissolved and deposited on the catalysts during continuous electrochemical tests [52]. Thus, a graphite rod was utilized as the counter electrode when conducting the stability study. Fig. 4C shows the polarization curves of Co_xP NPs/CC before and after 5000 CV scanning cycles in the potential range of −0.20 to +0.10 V *vs.* RHE. In contrast to the initial curve, an inappreciable distinction can be observed for the curve obtained after 5000 cycles. In addition, a long-time (at least 12 h) electrolysis at a controlled overpotential of 150 mV was also performed. The time-dependent current density curve is displayed in Fig. 4D, and an acceptable damping is observed with a graphite rod used as the counter electrode. The corresponding current density is about 50 mA cm^{-2} (Fig. 4A) over overpotential of 150 mV, it is worth mentioning that the current density of 50 mA cm^{-2} is a relatively large value in robustness tests among most reported studies [53,54]. All the above results demonstrate that the as-prepared Co_xP NPs/CC has a good stability in acidic solution and a potential possibility to practical application.

Since the improved catalytic activity is principally attributed to the Co_xP NPs with smaller size and the supported CC with the high surface area, it is necessary to evaluate the

Please cite this article as: Tao BX et al., Heterogeneous cobalt phosphides nanoparticles anchored on carbon cloth realizing the efficient hydrogen generation reaction, International Journal of Hydrogen Energy, https://doi.org/10.1016/j.ijhydene.2018.11.018

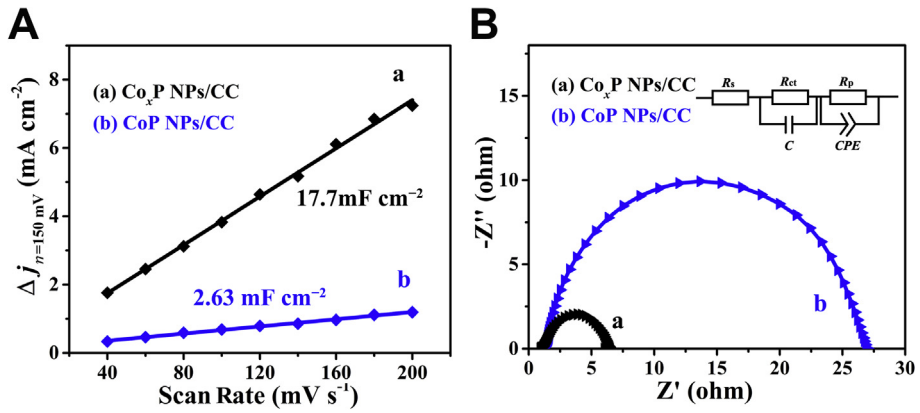

Fig. 5 – (A) Estimation of C_{dl} *via* plotting current density variation ($\Delta j = j_a$-j_c), at 150 mV *vs.* RHE, the data of which derived from CV plots. (B) Nyquist plots of electrochemical impedance spectra for CoP NPs/CC and Co_xP NPs/CC at a static overpotential of 100 mV. Inset: fitted equivalent circuit of Co_xP NPs/CC.

electrochemical active surface areas (ECSA) of the resultant electrocatalysts [55,56]. Hence we employed the CV scans to measure the electrochemical double layer capacitances (C_{dl}), in which a potential region without faradic current was chosen [57]. The CV curves at different scan rates were recorded in the range of +0.05 to +0.25 V (Fig. S7 A–C). Fig. 5A shows the capacitive current densities at +0.15 V as a function of scan rate for the Co_xP NPs/CC and CoP NPs/CC ($\Delta j = j_a - j_c$). The as-prepared Co_xP NPs/CC catalyst displays a C_{dl} value of 17.7 mF cm^{-2}, which is almost 6.7 times higher than that of pure phase CoP NPs/CC (2.63 mF cm^{-2}), demonstrating a comparatively larger ECSA of the resultant catalyst. In addition, the electrochemical impedance was studied at an overpotential of 100 mV, and the derived Nyquist plots and fitted equivalent circuit are exhibited in Fig. 5B. All the Nyquist plots of different samples exhibit only one legible semicircle in the high frequency region, which is closely related to the HER charge transfer kinetics [43,58]. The EIS data indicate that the Co_xP NPs/CC catalyst has a much lower charge transfer resistance (R_{ct}) than CoP NPs, suggesting a higher interfacial electron transport rate between electrocatalyst and electrolyte.

Conclusions

In summary, we have successfully designed an efficient HER electrocatalyst based on heterogeneous Co_xP NPs, namely both orthorhombic CoP and Co_2P existing in the resultant catalyst. Thanks to the weak reflux process and following low-temperature phosphatization procedure, the resultant Co_xP NPs with ultrafine size ensure more active sites exposed. Furthermore, the synergistic effect of the Co_2P and CoP in heterogeneous Co_xP NPs enhances the intrinsic catalytic property and charge-transfer rate in the HER process. In sulfuric acid medium, Co_xP NPs/CC exhibits the excellent HER catalytic performance, with a small overpotential (90 mV at 10 mA cm^{-2}), a low Tafel slope (67.9 mV dec^{-1}), a large exchange current density (0.58 mA cm^{-2}), and good durability. This work indicates that the intrinsic activity modifying to the catalysts play crucial roles in enhancing HER catalytic activity.

Acknowledgment

This work was financially supported by the Natural Science Foundation of Chongqing (No. CSTC-2015jcyjB50001) and the National Natural Science Foundation of China (No. 21675131).

Appendix A. Supplementary data

Supplementary data to this article can be found online at https://doi.org/10.1016/j.ijhydene.2018.11.018.

REFERENCES

[1] Li B, Setyawati M, Zou H, Dong J, Luo H, Li B, et al. Emerging 0D transition-metal dichalcogenides for sensors, biomedicine, and clean energy. Small 2017;13:1700527.
[2] Yu Z, Duan Y, Gao M, Lang C, Zheng Y, Yu S. A one-dimensional porous carbon-supported Ni/Mo_2C dual catalyst for efficient water splitting. Chem Sci 2017;8:968–73.
[3] Rodionova MV, Poudyal RS, Tiwari I, Voloshin RA, Zharmukhamedove SK, Nam HG, et al. Biofuel production: challenges and opportunities. Int J Hydrogen Energy 2017;42:8450–61.
[4] Najafpour MM, Fekete M, Sedigh DJ, Aro EM, Carpentier R, Eaton-Rye JJ, et al. Damage management in water-oxidizing catalysts: from photosystem II to nanosized metal oxides. ACS Catal 2015;5:1499–512.
[5] Yang Q, He Y, Fan Y, Chen X, Li Y. Efficient hydrogen evolution electrocatalysts from Li_x MoS_2 nanoparticles on three-dimensional substrate. Int J Hydrogen Energy 2017;42:6482–9.
[6] Najafpour MM, Renger G, Hołyńska M, Moghaddam AN, Aro EM, Carpentier R, et al. Manganese compounds as water-oxidizing catalysts: from the natural water-oxidizing complex to nanosized manganese oxide structures. Chem Rev 2016;116:2886–936.
[7] Li X, Liu W, Zhang M, Zhong Y, Weng Z, Mi Y, et al. Strong metal-phosphide interactions in core-shell geometry for enhanced electrocatalysis. Nano Lett 2017;17:2057–63.
[8] Najafpour MM, Salimi S, Nanosized RS. Manganese oxide supported on carbon black: a new, cheap and green

composite for water oxidation. Int J Hydrogen Energy 2017;42:255–64.
[9] Chen L, Yang W, Liu X, Jia J. Flower-like CoS_2/MoS_2 nanocomposite with enhanced electrocatalytic activity for hydrogen evolution reaction. Int J Hydrogen Energy 2017;42:12246–53.
[10] Zhan T, Liu X, Lu S, Hou W. Nitrogen doped NiFe layered double hydroxide/reduced graphene oxide mesoporous nanosphere as an effective bifunctional electrocatalyst for oxygen reduction and evolution reactions. Appl Catal B 2017;205:551–8.
[11] Wu Z, Li X, Liu W, Zhong Y, Gan Q, Li X, et al. Materials chemistry of iron phosphosulfide nanoparticles: synthesis, solid state chemistry, surface structure and electrocatalysis for hydrogen evolution reaction. ACS Catal 2017;7:4026–32.
[12] Zhang M, Ci S, Li H, Cai P, Xu H, Wen Z. Highly defective porous CoP nanowire as electrocatalyst for full water splitting. Int J Hydrogen Energy 2017;42:29080–90.
[13] Wang M, Ye C, Wang M, Lia T, Yu Y, Bao S. Synthesis of M (Fe_3C, Co, Ni)-porous carbon frameworks as high-efficient ORR catalysts. Energy Storage Materials 2018;11:112–7.
[14] Zhou X, Zhang Y. Noble metal-free hydrogen evolution catalysts for water splitting. Chem Soc Rev 2015;44:5148–80.
[15] Chan K, Hai X, Ye J. Transition metal disulfides as noble-metal-alternative co-catalysts for solar hydrogen production. Adv Energy Mater 2016;6:502555.
[16] Staszak-Jirkovsky J, Malliakas C, Lopes P, Danilovic N, Kota S, Chang K, et al. Design of active and stable Co-Mo-S_x chalcogels as pH-universal catalysts for the hydrogen evolution reaction. Nat Mater 2016;15:197–203.
[17] Liu P, Li J, Xiang B. Facile synthesis of NiS_2 nanowires and its efficient electrocatalytic performance for hydrogen evolution reaction. Int J Hydrogen Energy 2018;43:72–7.
[18] Gao L, Chen S, Zhang H, Zou Y, She X, Yang D, et al. Porous CoP nanostructure electrocatalyst derived from DUT-58 for hydrogen evolution reaction. Int J Hydrogen Energy 2018;43:13904–10.
[19] Hsu CL, Chang YH, Chen TY, Tseng CC, Wei KH, Li LJ. Enhancing the electrocatalytic water splitting efficiency for amorphous MoS_x. Int J Hydrogen Energy 2014;39:4788–93.
[20] Hu J, Huang B, Zhang C, Wang Z, An Y, Zhou D, et al. Engineering stepped edge surface structures of MoS_2 sheet stacks to accelerate the hydrogen evolution reaction. Energy Environ Sci 2017;10:593–603.
[21] Zhou W, Lu J, Zhou K, Yang L, Ke Y, Tang Z, et al. $CoSe_2$ nanoparticles embedded defective carbon nanotubes derived from MOFs as efficient electrocatalyst for hydrogen evolution reaction. Nano Energy 2016;28:143–50.
[22] Najafpour MM, Hosseini SM, Tavahodi M, Ghobadi MZ. The conversion of $CoSe_2$ to Co oxide under the electrochemical water oxidation condition. Int J Hydrogen Energy 2016;41:13469–75.
[23] Liu T, Sun X, Asiri AM, He Y. One-step electrodeposition of Ni-Co-S nanosheets film as a bifunctional electrocatalyst for efficient water splitting. Int J Hydrogen Energy 2016;41:7264–9.
[24] Yang Y, Zhang K, Lin H, Li X, Chan H, Yang L, et al. MoS_2-Ni_3S_2 heteronanorods as efficient and stable bifunctional electrocatalysts for overall water splitting. ACS Catal 2017;7:2357–66.
[25] Wang L, Li Y, Xia M, Li Z, Chen Z, Ma Z, et al. Ni nanoparticles supported on graphene layers: an excellent 3D electrode for hydrogen evolution reaction in alkaline solution. J Power Sources 2017;347:220–8.
[26] Chang J, Lv Q, Li G, Ge J, Liu C, Xing W. Core-shell structured $Ni_{12}P_5/Ni_3(PO_4)_2$ hollow spheres as difunctional and efficient electrocatalysts for overall water electrolysis. Appl Catal B 2017;204:486–96.
[27] Pu Z, Liu Q, Tang C, Asiri A, Sun X. Ni_2P nanoparticle films supported on a Ti plate as an efficient hydrogen evolution cathode. Nanoscale 2014;6:11031–4.
[28] McKone J, Sadtler B, Werlang C, Lewis N, Gray H. Ni-Mo nanopowders for efficient electrochemical hydrogen evolution. ACS Catal 2013;3:166–9.
[29] Yan H, Tian C, Wang L, Wu A, Meng M, Zhao L, et al. Phosphorus-modified tungsten nitride/reduced graphene oxide as a high-performance, non-noble-metal electrocatalyst for the hydrogen evolution reaction. Angew Chem Int Ed 2015;54:6325–9.
[30] Popczun E, Read C, Roske C, Lewis N, Schaak R. Highly active electrocatalysis of the hydrogen evolution reaction by cobalt phosphide nanoparticles. Angew Chem Int Ed 2014;26:5531–4.
[31] Wu T, Pi M, Zhang D, Chen S. Three-dimensional porous structural MoP_2 nanoparticles as a novel and superior catalyst for electrochemical hydrogen evolution. J Power Sources 2016;28:551–4.
[32] Ojha K, Sharma M, Kolev H, Ganguli AK. Reduced graphene oxide and MoP composite as highly efficient and durable electrocatalyst for hydrogen evolution in both acidic and alkaline media. Catal Sci Technol 2017;7:668–76.
[33] Cui W, Liu Q, Xing Z, Asiri A, Alamry K, Sun X. MoP nanosheets supported on biomass-derived carbon flake: one-step facile preparation and application as a novel high-active electrocatalyst toward hydrogen evolution reaction. Appl Catal B 2015;164:144–50.
[34] Pua Z, Wei S, Chen Z, Mu S. Flexible molybdenum phosphide nanosheet array electrodes for hydrogen evolution reaction in a wide pH range. Appl Catal B 2016;196:193–8.
[35] Ye C, Wang M, Chen G, Deng Y, Li L, Luo H, et al. One-step CVD synthesis of carbon framework wrapped Co_2P as flexible electrocatalyst for efficient hydrogen evolution. J Mater Chem A 2017;5:7791–5.
[36] Qiu H, Ito Y, Cong W, Tan Y, Liu P, Hirata A, et al. Nanoporous graphene with single-atom nickel dopants: an efficient and stable catalyst for electrochemical hydrogen production. Angew Chem Int Ed 2015;54:14031–5.
[37] Callejas J, Read C, Popczun E, McEnaney J, Schaak R. Nanostructured Co_2P electrocatalyst for the hydrogen evolution reaction and direct comparison with morphologically equivalent CoP. Chem Mater 2015;27:3769–74.
[38] Liu M, Li J. Cobalt phosphide hollow polyhedron as efficient bifunctional electrocatalysts for the evolution reaction of hydrogen and oxygen. ACS Appl Mater Interfaces 2016;8:2158–65.
[39] Jiang P, Liu Q, Ge C, Cui W, Pu Z, Asiri A, et al. CoP nanostructures with different morphologies: synthesis, characterization and a study of their electrocatalytic performance toward the hydrogen evolution reaction. J Mater Chem A 2014;2:14634–40.
[40] Liang Y, Li Y, Wang H, Zhou J, Wang J, Regier T, et al. Co_3O_4 nanocrystals on graphene as a synergistic catalyst for oxygen reduction reaction. Nat Mater 2011;10:780–6.
[41] Ma L, Shen X, Zhou H, Zhu G, Ji Z, Chen K. CoP nanoparticles deposited on reduced graphene oxide sheets as an active electrocatalyst for the hydrogen evolution reaction. J Mater Chem A 2015;3:5337–43.
[42] Yi S, Yan J, Wulan B, Li S, Liu K, Jiang Q. Noble-metal-free cobalt phosphide modified carbon nitride: an efficient photocatalyst for hydrogen generation. Appl Catal B 2017;200:477–83.
[43] Zhang G, Wang G, Liu Y, Liu H, Qu J, Li J. Highly active and stable catalysts of phytic acid-derivative transition metal phosphides for full water splitting. J Am Chem Soc 2016;138:14686–93.

Please cite this article as: Tao BX et al., Heterogeneous cobalt phosphides nanoparticles anchored on carbon cloth realizing the efficient hydrogen generation reaction, International Journal of Hydrogen Energy, https://doi.org/10.1016/j.ijhydene.2018.11.018

[44] Sun Y, Gao S, Lei F, Liu J, Liang L, Xie Y. Atomically-thin non-layered cobalt oxide porous sheets for highly efficient oxygen-evolving electrocatalysts. Chem Sci 2014;5:3976–82.
[45] Das D, Nanda K. One-step, integrated fabrication of Co_2P nanoparticles encapsulated N, P dual-doped CNTs for highly advanced total water splitting. Nano Energy 2016;30:303–11.
[46] Li X, Fang Y, Li F, Tian M, Long X, Jin J, et al. Ultrafine Co_2P nanoparticles encapsulated in nitrogen and phosphorus dual-doped porous carbon nanosheet/carbon nanotube hybrids: high-performance bifunctional electrocatalysts for overall water splitting. J Mater Chem A 2015;4:15501–10.
[47] Hou C, Cao S, Fu W, Chen Y. Ultrafine CoP nanoparticles supported on carbon nanotubes as highly active electrocatalyst for both oxygen and hydrogen evolution in basic media. ACS Appl Mater Interfaces 2015;7:28412–9.
[48] Dong Y, Kong L, Wang G, Jiang P, Zhao N, Zhang H. Photochemical synthesis of Co_xP as cocatalyst for boosting photocatalytic H_2 production via spatial charge separation. Appl Catal B 2017;211:245–51.
[49] Tian L, Yan X, Chen X, Liu L, Chen X. One-pot, large-scale, simple synthesis of Co_xP nanocatalysts for electrochemical hydrogen evolution. J Mater Chem A 2016;4:13011–6.
[50] Dong G, Fang M, Wang H, Yip S, Cheung H, Wang F, et al. Insight into the electrochemical activation of carbon-based cathodes for hydrogen evolution reaction. J Mater Chem A 2015;3:13080–6.
[51] Shi Y, Zhang B. Recent advances in transition metal phosphide nanomaterials: synthesis and applications in hydrogen evolution reaction. Chem Soc Rev 2016;45:1529–41.
[52] Chen R, Yang C, Cai W, Wang H, Miao J, Zhang L, et al. Use of platinum as the counter electrode to study the activity of nonprecious metal catalysts for the hydrogen evolution reaction. ACS Energy Lett 2017;2:1070–5.
[53] Xu K, Wang F, Wang Z, Zhan X, Wang Q, Cheng Z, et al. Component-controllable $WS_{2(1-x)}Se_{2x}$ nanotubes for efficient hydrogen evolution reaction. ACS Nano 2014;8:8468–76.
[54] Fang Z, Peng L, Qian Y, Zhang X, Xie Y, Cha JJ, et al. Dual tuning of Ni-Co-A (A = P, Se, O) nanosheets by anion substitution and holey engineering for efficient hydrogen evolution. J Am Chem Soc 2018;140:5241–7.
[55] Song F, Hu X. Ultrathin cobalt-manganese layered double hydroxide is an efficient oxygen evolution catalyst. J Am Chem Soc 2014;136:16481–4.
[56] Sivanantham A, Shanmugam S. Nickel selenide supported on nickel foam as an efficient and durable non-precious electrocatalyst for the alkaline water electrolysis. Appl Catal B 2017;203:485–93.
[57] Wang H, Lu Z, Kong D, Sun J, Hymel T, Cui Y. Electrochemical tuning of MoS_2 nanoparticles on three-dimensional substrate for efficient hydrogen evolution. ACS Nano 2014;8:4940–7.
[58] Deng C, Ding F, Li X, Guo Y, Ni W, Yan H, et al. Templated-preparation of a three-dimensional molybdenum phosphide sponge as a high performance electrode for hydrogen evolution. J Mater Chem A 2016;4:59–66.

Please cite this article as: Tao BX et al., Heterogeneous cobalt phosphides nanoparticles anchored on carbon cloth realizing the efficient hydrogen generation reaction, International Journal of Hydrogen Energy, https://doi.org/10.1016/j.ijhydene.2018.11.018